A study on the method of fundamental solutions using the image concept

Jhen-Jyun Tsai[1*], Hung-Chih Shieh[1], Jia-Wei Lee[1], Jeng-Tzong Chen[1, 2]

[1]Department of Harbor and River Engineering
[2]Department of Mechanical and Mechatronic Engineering
National Taiwan Ocean University
Keelung 20224, Taiwan
[*]M97520026@mail.ntou.edu.tw

NSC PROJECT: NSC98-2221-E-019-017-MY3

ABSTRACT

In this paper, analytical and semi-analytical numerical solutions for Green's functions are obtained by using the image method which can be seen as a special method of fundamental solutions (MFS). The image method is employed to solve the Green's function for the annular, eccentric and half-plane Laplace problems. In addition, an analytical solution is derived for the fixed-free annular case. For the half-plane problem with a circular hole and an eccentric annulus, semi-analytical solutions are both obtained by using the image concept after determining the strengths of two frozen image points and a free constant by matching boundary conditions. It is found that two frozen images terminated at the two focuses in the bipolar coordinates for the problems with two circular boundaries. A boundary value problem of an eccentric annulus without sources is also considered. Error distribution is plotted after comparing with the analytical solutions derived by Lebedev *et al.* using the bipolar coordinates. The optimal locations for the source distribution in the MFS are also examined by using the image concept. It is observed that we should locate singularities on the two focuses to obtain better results in the MFS. Besides, whether the free constant is required or not in the MFS is also studied. The results are compared well with the analytical solutions.

Keywords: method of fundamental solutions, image method, Green's function, boundary value problem.

1. Introduction

Method of fundamental solutions (MFS) has been developed for more than 50 years. The method was proposed by Kupradze and Aleksidze [1] in 1964 in Russia. In the potential theory, it is well known that the MFS can solve potential problems if fundamental solutions of the partial differential equation are given. The Green's function has been studied and applied in many fields by mathematicians as well as engineers [2] in 1977. For the image method, Thomson [3] proposed the concept of reciprocal radii to find the image source to satisfy the homogeneous boundary condition. Chen and Wu [4] proposed an alternative way to find the location of image by employing the degenerate kernel. The Green's function of a circular ring has been solved using the complex variable by Courant and Hilbert [5]. The Green's function of Laplace equation was obtained by using the image method for a simple case in the Greenberg's book [6]. To derive the Green's function for problems with circular boundaries by using the image method is the main concern of this paper. Here, we put singularities along the radial direction in the method of image in stead of angular distributions for the annular case.

In this paper, both analytical and semi-analytical solutions for the Green's functions of annular, eccentric and half-plane problems are derived. The analytical solutions for the fixed-free annulus are obtained by using the MFS in conjunction with the addition theorem or the so-called degenerate kernel. For the semi-analytical solution, a half-plane problem with a circular cavity and an eccentric annulus are considered to demonstrate that the image method can capture the optimal location of MFS sources. The agreement between the semi-analytical solution and null-field boundary integral equation method (BIEM) is examined. Following the successful experiences on the derivation of Green's function, we extend to solve the boundary value problem without sources by using the MFS. Saavedra and Power [7] have discussed the role of free constant in the MFS. As quoted by [7], "*However, usually it is necessary to add a constant term in particular in two dimensions, where it is required for completeness purposes. As can be observed a constant value is always a solution of the Laplace's equation.* "Whether it is necessary for adding the constant in the MFS formulation is a nontrivial issue. It is interesting to find that only the strengths at the two focuses for the eccentric annulus are required, if the rigid body term is considered in the MFS. When the conventional MFS without adding a constant term is used, how to represent the constant field by superimposing the singularities becomes an interesting issue. Error distribution is plotted after comparing with the analytical solutions of Lebedev *et al.*[8]. The optimal location in the MFS highly correlates to the two focuses for the problem of eccentric annulus. Numerical results of eccentric case are compared with the analytical solution using the bipolar coordinates.

2. An analytical solution for the Green's function of annular region by using the image method

For a two-dimensional annular problem as shown in Fig. 1, the Green's function satisfies

$$\nabla^2 G(x,\zeta) = \delta(x-\zeta)\,, \quad x \in \Omega\,, \tag{1}$$

where Ω is the domain of interest and δ denotes the Dirac-delta function for the source at ζ. For simplicity, the Green's function is considered to be subject to the fixed-free boundary conditions

$$G(x,\zeta) = 0\,, \quad x \in B_1\,, \tag{2}$$

$$\frac{\partial G(x,\zeta)}{\partial n_x} = 0\,, \quad x \in B_2\,, \tag{3}$$

where B_1 and B_2 are the inner and outer boundaries, respectively. As mentioned in Courant and Hilbert [5], the interior and exterior Green's functions can satisfy the fixed-free boundary conditions if the image source is correctly selected. The closed-form Green's functions for both interior and exterior problems are written to be the same form

$$G(x,\zeta) = \ln|x-\zeta| - \ln|x-\zeta'| + \ln a - \ln R_\zeta\,,\; x \in \Omega\,, \tag{4}$$

where a is the radius of the circle, $\zeta = (R_\zeta, 0)$, R_ζ is the distance from the source to the center of the circle, ζ' is the image source and its position is at $(a^2/R_\zeta, 0)$ as shown in Fig. 2.

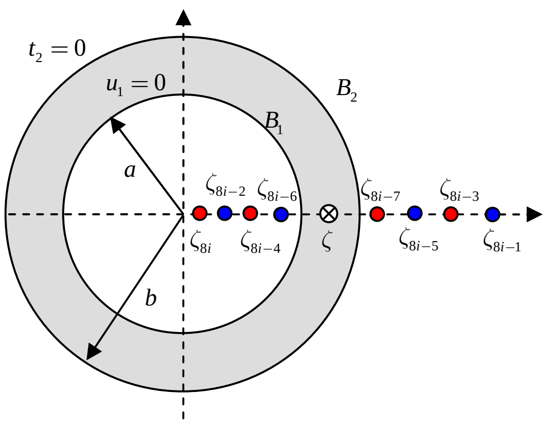

Fig. 1 Sketch of an annular problem.

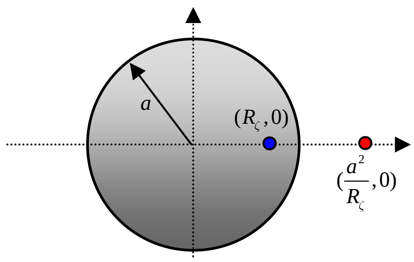

(a) Interior problem

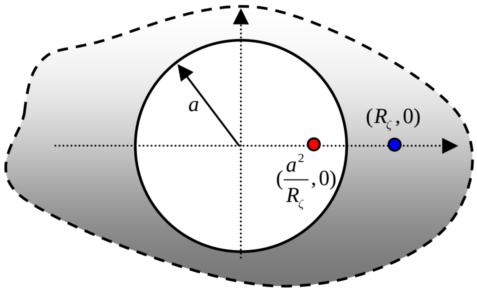

(b) Exterior problem

Fig. 2 Sketch of image location (a) Interior case, and (b) Exterior case.

Figure 1 depicts a series of images for the annular problems. We consider the fundamental solution $U(x,s)$ for each source singularity which satisfies

$$\nabla^2 U(x,s) = 2\pi\delta(x-s)\,. \tag{5}$$

Then, we obtain the fundamental solution as follows:

$$U(x,s) = \ln r\,, \tag{6}$$

where r is the distance between s and x ($r \equiv |x-s|$). Based on the separable property of addition theorem or degenerate kernel, the fundamental solution $U(x,s)$ can be expanded into series form by separating the field point $x(\rho,\phi)$ and source point $s(R,\theta)$ in the polar coordinates [4]:

$$U(x,s) = \begin{cases} U^I(\rho,\phi;R,\theta) = \ln R \\ \qquad -\sum_{m=1}^{\infty} \frac{1}{m}\left(\frac{\rho}{R}\right)^m \cos m(\theta-\phi),\; R \geq \rho, \\ U^E(\rho,\phi;R,\theta) = \ln \rho \\ \qquad -\sum_{m=1}^{\infty} \frac{1}{m}\left(\frac{R}{\rho}\right)^m \cos m(\theta-\phi),\; R < \rho, \end{cases} \tag{7}$$

where the superscripts of I and E denote the interior and exterior regions, respectively.

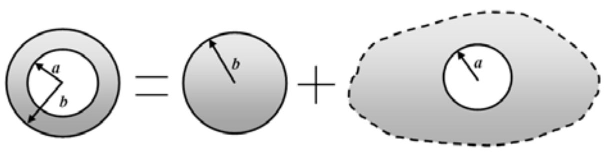

(a) Interior problem (b) Exterior problem

Fig. 3 An annular case composed of (a) Interior and (b) Exterior cases.

Now let us extend a circular case to an annular case. An annular case can be seen as a combination of interior and exterior problems as shown in Fig. 3. By matching the fixed-free boundary conditions for the inner and outer boundaries, we introduce image points ζ_1 and ζ_2, respectively. Since ζ_2 results in the nonhomogeneous boundary conditions on the outer boundary, we need to introduce an extra image point ζ_3. Similarly, ζ_1 results in the nonhomogeneous boundary conditions on the inner boundary and an additional image point ζ_4 is also required. By repeating the same procedure, we have a series of image sources locating at

$$\begin{aligned}
&\zeta_{8i-7}=\frac{b^2}{R_\zeta}\left(\frac{b^4}{a^4}\right)^{i-1},\ \zeta_{8i-5}=\frac{b^2R_\zeta}{a^2}\left(\frac{b^4}{a^4}\right)^{i-1},\\
&\zeta_{8i-3}=\frac{b^4}{a^2R_\zeta}\left(\frac{b^4}{a^4}\right)^{i-1},\ \zeta_{8i-1}=\frac{b^4R_\zeta}{a^4}\left(\frac{b^4}{a^4}\right)^{i-1},\ i\in N,
\end{aligned}\tag{8}$$

$$\begin{aligned}
&\zeta_{8i-6}=\left(\frac{a^2}{R_\zeta}\right)\left(\frac{a^4}{b^4}\right)^{i-1},\ \zeta_{8i-4}=\frac{a^2R_\zeta}{b^2}\left(\frac{a^4}{b^4}\right)^{i-1},\\
&\zeta_{8i-2}=\left(\frac{a^4}{b^2R_\zeta}\right)\left(\frac{a^4}{b^4}\right)^{i-1},\ \zeta_{8i}=\frac{a^4R_\zeta}{b^4}\left(\frac{a^4}{b^4}\right)^{i-1},\ i\in N.
\end{aligned}\tag{9}$$

Following the successive image process, it is found that the final two image locations freeze at the origin and infinity. There are two strengths of singularities to be determined. Therefore, the total Green's function is rewritten as

$$\begin{aligned}
G(x,\zeta)=\frac{1}{2\pi}\Big\{&\Big[\ln|x-\zeta|+\lim_{N\to\infty}\Big[\sum_{i=1}^{N}\big(\ln|x-\zeta_{8i-7}|\\
&-\ln|x-\zeta_{8i-6}|-\ln|x-\zeta_{8i-5}|-\ln|x-\zeta_{8i-4}|\big)\\
&-\ln|x-\zeta_{8i-3}|+\ln|x-\zeta_{8i-2}|+\ln|x-\zeta_{8i-1}|\\
&+\ln|x-\zeta_{8i}|\Big]+c(N)\ln\rho+e(N)\Big]\Big\},
\end{aligned}\tag{10}$$

where $c(N)$ and $e(N)$ are the unknown coefficients which may be analytically and numerically determined by matching the inner and outer boundary conditions. To match the outer free boundary condition, normal boundary derivative of Eq. (10) yields

$$\begin{aligned}
\frac{\partial G(x,\zeta)}{\partial n_x}=\frac{1}{2\pi}\frac{\partial}{\partial n_x}\Big\{&\Big[\ln|x-\zeta|+\lim_{N\to\infty}\Big[\sum_{i=1}^{N}\big(\ln|x-\zeta_{8i-7}|\\
&-\ln|x-\zeta_{8i-6}|-\ln|x-\zeta_{8i-5}|-\ln|x-\zeta_{8i-4}|\big)\\
&-\ln|x-\zeta_{8i-3}|+\ln|x-\zeta_{8i-2}|+\ln|x-\zeta_{8i-1}|\\
&+\ln|x-\zeta_{8i}|\Big]+c(N)\ln\rho+e(N)\Big]\Big\}.
\end{aligned}\tag{11}$$

By substituting the inner and outer boundary conditions into Eq. (10) and Eq. (11) and using the addition theorem (degenerate kernel), the analytical forms of $c(N)$ and $e(N)$ are obtained as

$$\begin{Bmatrix} c(N) \\ e(N) \end{Bmatrix}=\begin{Bmatrix} -1 \\ \ln a-\ln R_\zeta \end{Bmatrix}.\tag{12}$$

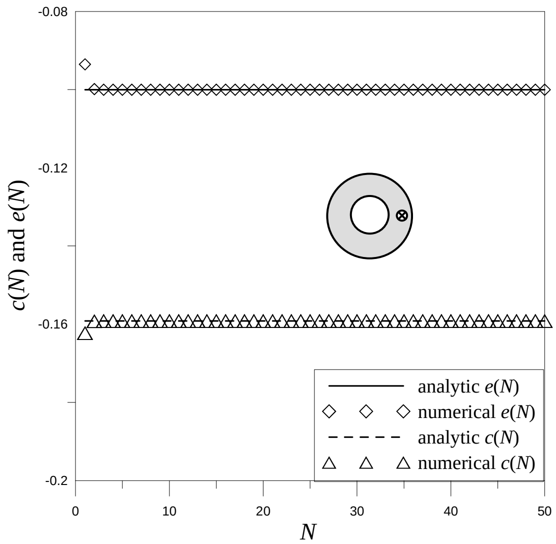

(a) annular case

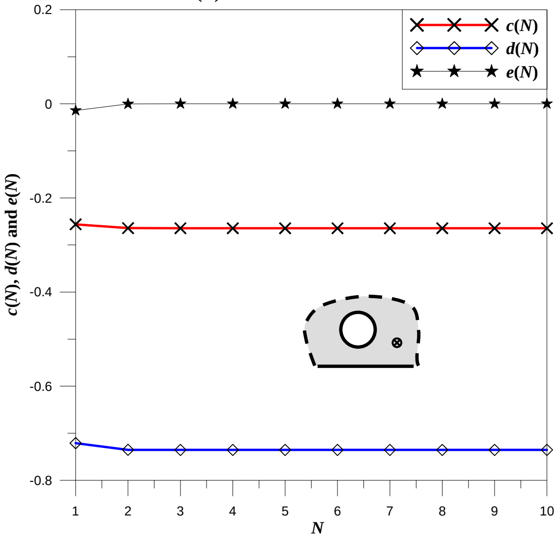

(b) half-plane case

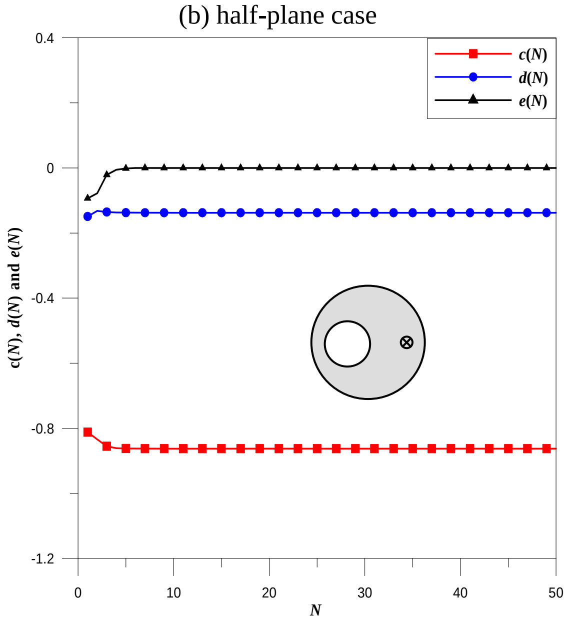

(c) eccentric case

Fig. 4 Values of $c(N)$, $d(N)$ and $e(N)$. (a) annular case, (b) half-plane case, (c) eccentric case.

Numerically speaking, the values of unknown $c(N)$ and $e(N)$ can be alternatively determined by matching the inner and outer boundary conditions attwo selected collocation points. The obtained numerical values of $c(N)$ and $e(N)$ agree well with the analytical result of Eq. (12) as shown in Fig. 4(a).

3. Semi-analytical solutions for the half-plane problem with a circular hole and the eccentric ring by using the image method

Following the success of annular case for the iterative images, we now extend to the half-plane problem with a circular hole as shown in Fig. 5. In a similar way of finding the image for matching the inner circular boundary condition as the annular case, an image is found. Besides, the reflection image point is given to match the ground surface. However, the two additional images, one inside the hole and the other under the ground line, result in new images to match the boundary condition of ground surface and inner circle, respectively. The iterative images and their locations are shown in Fig. 5. Two frozen images are found as the number of images becomes infinity. The locations of two frozen images are governed by

$$R_c = \frac{a^2}{R_d},\ \ R_d = 2b - R_c, \tag{13}$$

where a, b, R_c and R_d are shown in Fig. 5. Therefore, the Green's function is represented by

$$\begin{aligned} G(x,\zeta) = \frac{1}{2\pi}\Big\{ &\ln|x-\zeta| - \lim_{N\to\infty}\Big[\sum_{i=1}^{N}\big(\ln|x-\zeta_{4i-3}| \\ &+\ln|x-\zeta_{4i-2}| - \ln|x-\zeta_{4i-1}| - \ln|x-\zeta_{4i}|\big) \\ &+c(N)\ln|x-\zeta_c| + d(N)\ln|x-\zeta_d| + e(N)\Big]\Big\}, \end{aligned} \tag{14}$$

where ζ_c and ζ_d are the location of the final two images, $c(N)$, $d(N)$ and $e(N)$ need to be determined by matching the boundary conditions. Based on the idea of MFS, we can say that not only some MFS sources are optimally located by using the image method but also the strengths except the two frozen images are also determined. Only three unknown coefficients are required to be determined by matching the boundary condition. Numerical values for $c(N)$, $d(N)$, $e(N)$ versus N are shown in Fig. 4(b). The contour plots by using the present method and the null-field BIE [9] are shown in Fig. 6. It is found that good agreement is made after comparing our result with that of the null-field BIE.

Instead of using the conventional MFS as shown in Fig. 7, this image method can be seen as a special case of MFS with optimal location of sources. Besides, the strengths of all the singularities are determined in advance except the singularity strengths of the two frozen images and one free constant.

Similarly, we can extend the semi-analytical approach to solve the Green's function of eccentric case. The final locations of two image points are governed by

$$R_c = \frac{b^2}{R_d - e} + e,\ \ R_d = \frac{a^2}{R_c}, \tag{15}$$

where a, b, e, R_c and R_d are shown in Fig. 8. The two analytical frozen images (ζ_c and ζ_d) are shown in Fig. 8 and the numerical experiment also supports this result.

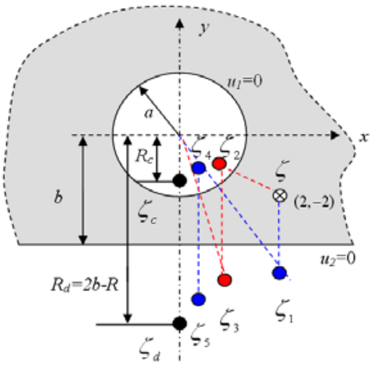

Fig. 5 A half-plane problem with a circular hole and its images.

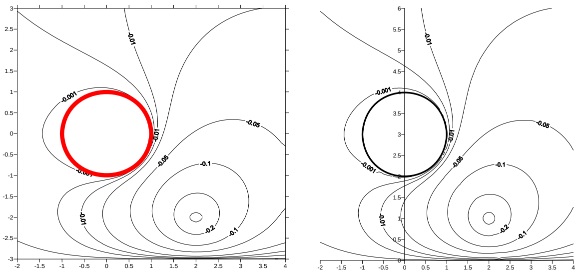

(a) image method (b) null-field BIE

Fig. 6 Contour plots by using (a) image method and (b) null-field BIE.

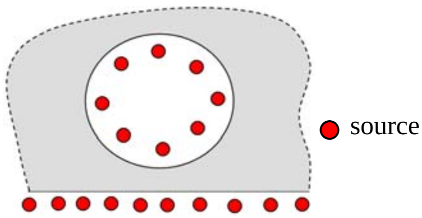

Fig. 7 Conventional MFS.

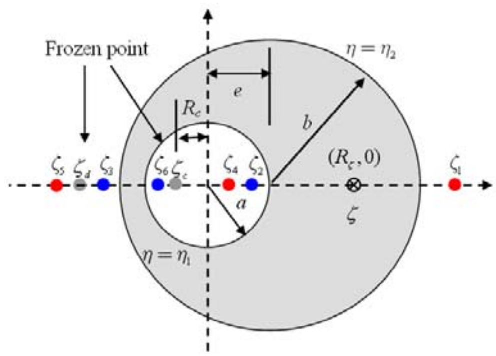

Fig. 8 Sketch of an eccentric problem subject to a concentrated load and the final two images at ζ_c and ζ_d.

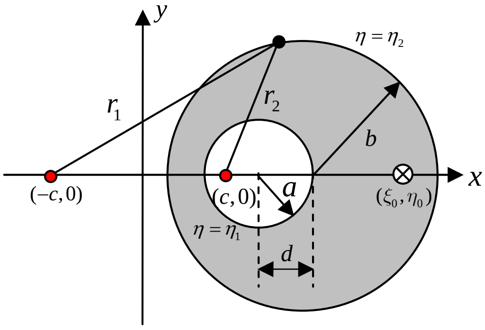

Fig. 9 Geometry relation of the bipolar coordinates.

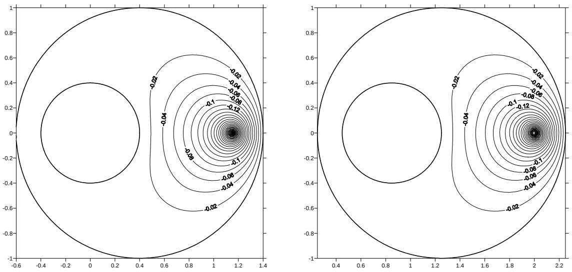

(a) image method (b) bipolar coordinates

Fig. 10 Contour plots for the eccentric solutions by using (a) image method and (b) analytical solution using the bipolar coordinates.

Numerical values for $c(N)$, $d(N)$, $e(N)$ versus N are shown in Fig. 4(c). The analytical solution of series form in the bipolar coordinates was derived by Heyda [10] as shown below:

$$G_1(\xi,\eta;\xi_0,\eta_0)=\begin{cases} \frac{1}{2\pi}\Big[\frac{(\eta_1-\eta)(\eta_0-\eta_2)}{\eta_1-\eta_2} \\ +2\sum_{n=1}^{\infty}\frac{\sinh n(\eta_1-\eta)\sinh n(\eta_0-\eta_2)}{n\sinh n(\eta_1-\eta_2)} \\ \cos n(\xi-\xi_0)\Big],\ \eta_1<\eta<\eta_0, \\ \frac{1}{2\pi}\Big[\frac{(\eta-\eta_2)(\eta_1-\eta_0)}{\eta_1-\eta_2} \\ +2\sum_{n=1}^{\infty}\frac{\sinh n(\eta_1-\eta_0)\sinh n(\eta-\eta_2)}{n\sinh n(\eta_1-\eta_2)} \\ \cos n(\xi-\xi_0)\Big],\ \eta_0<\eta<\eta_2, \end{cases} \quad (16)$$

where (ξ,η) is the bipolar coordinates, $\eta=\eta_1$ and $\eta=\eta_2$ denote the inner and outer circles, respectively and (ξ_0,η_0) is the position of source point as shown in Fig. 9. The contour plots by using the present method and the analytical solution are shown in Fig. 10. Good agreement is observed.

4. Numerical solutions for an eccentric annulus without sources by using the MFS

In the foregoing section, we have derived the Green's function of an eccentric case. In this section, we solve boundary value problems without sources by using the MFS as shown in Fig. 11. The solution of MFS is written as

$$u(x)=\sum_{j=1}^{N}d_j U(x,s_j), \quad (17)$$

where N is the number of source points, d_j is the j^{th} unknown coefficient. By matching the Dirichlet boundary conditions for the inner and outer boundaries, we can determine the unknown coefficients of d_j.

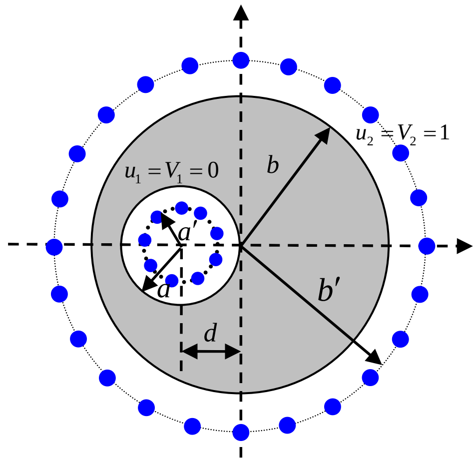

Fig. 11 Sketch of an eccentric annulus without sources.

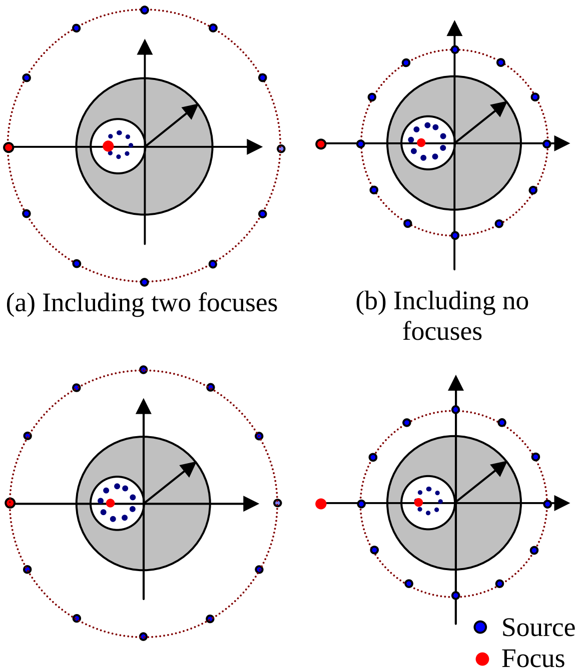

(a) Including two focuses (b) Including no focuses

(c) Including the left (outer) focus (d) Including the right (inner) focus

Fig. 12 Sketch of the source distribution in the MFS (a) including two focuses (b) including no Focuses (c) including the left (outer) focus (d) including the right (inner) focus.

In the above cases for deriving the Green's function, we find that there are two frozen points by using the image method which locate on the two focuses in the bipolar coordinates. We suppose that the two frozen locations may also be very important for problems without sources. Here, we solve boundary value problems of eccentric cases by using the MFS. The pattern of source distribution is shown in Fig. 12 for (a) including two focuses, (b) including no focuses, (c) including the left (outer) focus and (d) including the right (inner) focus, respectively. The solutions of the MFS are compared with the analytical solution derived by Lebedev *et al.*[8]. The analytical solution of eccentric case obtained by using the bipolar coordinates is given below:

$$u(\xi,\eta) = A\eta + B = A(\ln r_1 - \ln r_2) + B\,, \qquad (18)$$

where

$$A = \frac{V_1 - V_2}{\sinh^{-1}\left(\frac{c}{a}\right) - \sinh^{-1}\left(\frac{c}{b}\right)}\,, \qquad (19)$$

$$B = V_1 - \frac{V_1 - V_2}{\sinh^{-1}\left(\frac{c}{a}\right) - \sinh^{-1}\left(\frac{c}{b}\right)} \sinh^{-1}\left(\frac{c}{a}\right), \qquad (20)$$

$$c = \frac{\sqrt{a^4 - 2a^2b^2 + b^4 - 2a^2d^2 - 2b^2d^2 + d^4}}{2d}. \qquad (21)$$

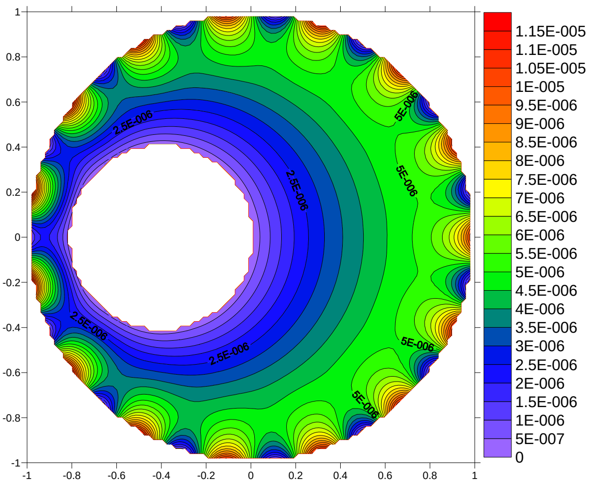

(a) Including the two focuses (-2,0), (-0.5,0).

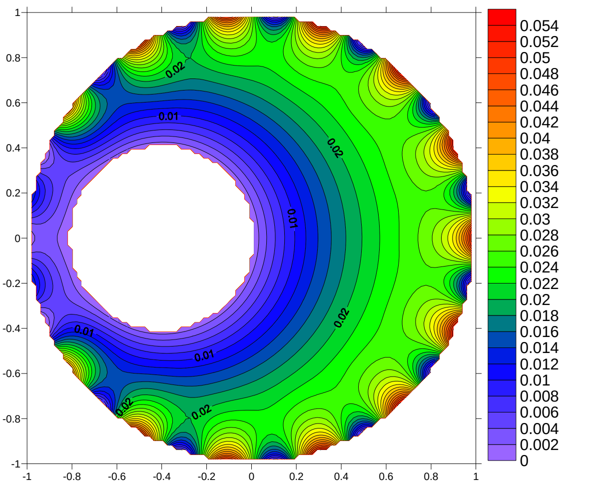

(b) Including no the two focuses.

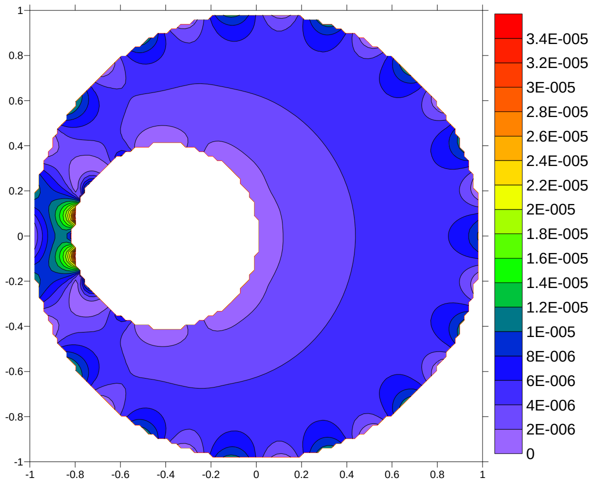

(c) Including the left (outer) focus (-2,0).

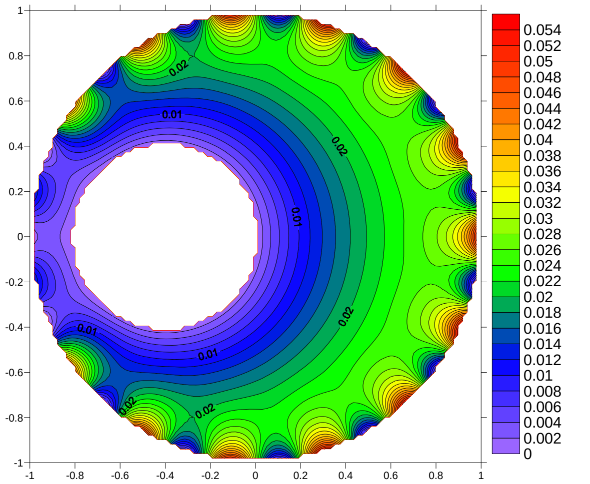

(d) Including the right (inner) focus (-0.5,0).

Fig. 13 Error distribution of source locations (a) including the two focuses (-2,0), (-0.5,0) (b) including no the two focuses (c) including the left (outer) focus (-2,0) (d) including the right (inner) focus (-0.5,0).

Error distribution is defined by

$$\varepsilon(x) = \left\| u^N(x) - u^{exact}(x) \right\|,\ x \in D\,, \qquad (22)$$

and is shown in Fig. 13 for source locations (a) including the two focuses $(-2,0)$, $(-0.5,0)$, (b) not including the two focuses, (c) including one focus only $(-2,0)$ and (d) including one focus only $(-0.5,0)$, respectively. When the locations of sources include two focuses in Fig. 13(a), we find that the numerical result best matches the analytical solution.

In the analytical solution of Eq. (18), there exists a rigid body term, *B*. For the MFS, Saavedra and Power [7] have pointed out that a free constant is needed in the MFS for 2-D problems. Therefore, Eq. (17) is changed to

$$u(x) = \sum_{j=1}^{N} c_j U(x, s_j) + c_0\,, \qquad (23)$$

where c_0 is the free constant and c_j is the unknown coefficient. When the singularities along the two rings contain at the two focuses as shown in Fig. 12(a), we find that only the two nonzero strengths (c_1 and c_{16}) of singularities at the two focuses and the strength (c_0) happen to be equal to the coefficient of analytical solutions of Eqs. (19) and (20) and other weightings are all zeros, as shown in Fig. 14. The strengths of the two nonzero singularities are opposite to each other ($c_1 = -c_{16}$) as predicted by Eq. (18). This result can be analytically predicted. It indicates that we can approach the exact solution if the source locations of MFS are geniously chosen.

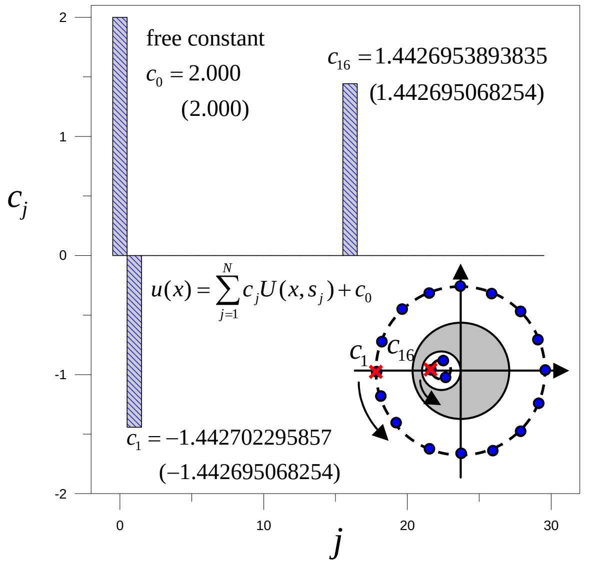

Fig. 14 Coefficient of c_j versus j by using Eq. (23) with a free constant, data in ( ) denotes the analytical solution.

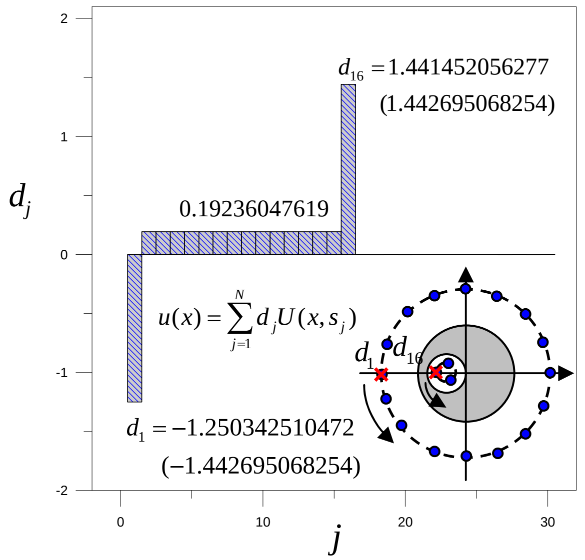

Fig. 15 Coefficient of d_j versus j by using Eq. (17) without a free constant.

Unfortunately, the conventional MFS always employed Eq. (17) instead of Eq. (23). The key difference is a free constant. Figure 15 shows that all singularities strengths in the inner sources are zeros except the one on the inner focus. If we use Eq. (17) free of a constant term, it is interesting to find the strengths (d_1~d_{15}) of outer singularities are all nonzero and only one nonzero singularity (d_{16}) on the interior focus for inner singularities. It is interesting to find that the difference (d_j-c_j) of Fig. 14 (c_j) and Fig. 15 (d_j) can represent a constant field of c_0=2 as shown in Fig. 16. This result indicates that a constant interior field (c_0) can be superimposed by using outer instead of inner singularities when the MFS solution of Eq. (17) does not contain the constant term. In Fig. 17, error distribution of Eq. (22) using MFS of Eq. (23) shows more accurate result than that using Eq. (17), because Eq. (23) approaches the analytical solution better than Eq. (17) does.

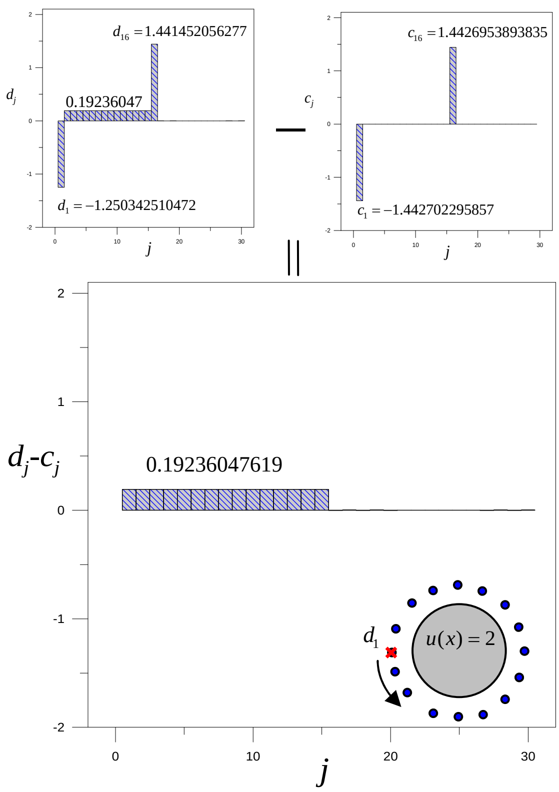

Fig. 16 Coefficient of d_j-c_j versus j to represent the constant field, $u(x)$=2.

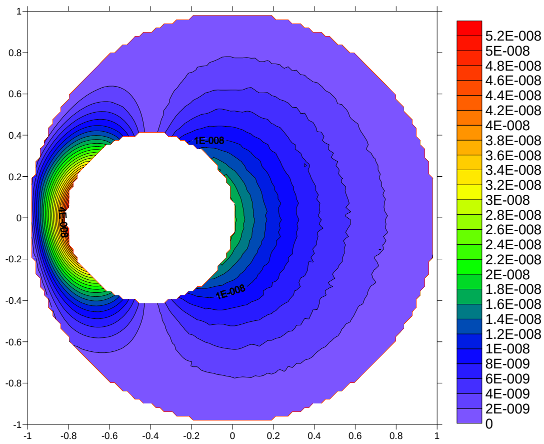

Fig. 17 Error distribution of source locations including the two focuses (-2,0), (-0.5,0) by using Eq. (23).

5. Conclusions

In this paper, the analytical and semi-analytical solutions for the Green's functions of annulus and half-plane problems were obtained by using the image method. The numerical solutions for boundary value problems of an eccentric annulus were obtained by using the MFS. For the analytical solution of annular case, the image method (a special MFS) was employed to solve the analytical Green's function of fixed-free annulus. For the half-plane problem with a circular cavity, a semi-analytical solution was obtained by determining only one free constant and two strengths of singularities at the two frozen images. Agreement is observed after comparing with the result of null-field BIEM. Besides, the same idea of semi-analytical approach was successfully extended to solve the Green's function in the eccentric annulus. The semi-analytical results also agree well with the analytical solution by using the bipolar coordinates. The numerical solution of an eccentric annulus without the source was compared with analytical solutions. The MFS with and without adding a constant were employed to solve the eccentric annulus without a source. It is found that only two nonzero singularities at the focuses and one constant are required to represent the analytical solution of eccentric annulus if MFS with an adding constant is used. Even though the MFS without adding a constant is employed to solve the solution, acceptable results can also be obtained. The reason can be explained that a constant term can be superimposed by using outer uniform singularities. In the demonstrated example, the addition of free constant is not absolutely necessary according to the numerical experiments. However, the MFS including the free constant yields the best solution in test example.

6. Acknowledgement

This research was partially supported by the National Science Council of Taiwan through Grant NSC 98-2221-E-019-017-MY3.

7. References

[1] V.D. Kupradze and M.A. Aleksidze, "A method for the approximate solution of limiting problems in mathematical physics," *Computational Mathematics Phyics*, vol. 4, pp. 199-205, 1964.
[2] M.A. Jaswon and G.T. Symm, *Integral Equation Methods in Potential Theory and Electrostatics*, Academic Press, New York; 1977.
[3] W. Thomson, "Maxwell in his treatise," *quotes a paper in the Cambridge and Dublin Math*., Vol. I., Chap. XI, 1848.
[4] J.T. Chen and C.S. Wu, "Alternative derivations for the Poisson integral formula," *International Journal of Mathematical Education in Science and Technology*, vol. 37, pp. 165-185, 2006.
[5] R. Courant and D. Hilbert, *Methods of Mathematical Physics*, Interscience, New York; 1953.
[6] M.D. Greenberg, *Application of Green's Functions in Science and Engineering*, Prentice-Hill, New Jersey; 1971.
[7] I. Saavedra and H. Power, "Multipole fast algorithm for the least-squares approach of the method of fundamental solutions for three-dimensional harmonic problems," *Numer Methods Partial Differ Equ*, vol. 19, pp. 825-845, 2003.
[8] N.N. Lebedev, I.P. Skalskaya and Y.S. Uflyand, *Worked Problems in Applied Mathematics*, Dover Publications, New York; 1979.
[9] J.T. Chen, K.H. Chou and S.K. Kao, "Derivation of Green's function using addition theorem," *Mechanics Research Communications*, vol. 36, pp. 351-363, 2009.
[10] J.F. Heyda, "A Green's function solution for the case of laminar incompressible flow between non-concentric circular cylinders," *Journal of The Franklin Institute*, vol. 267, pp. 25-34, 1959.

映像法於基本解法之研究

蔡振鈞[1]、謝宏治[1]、李家瑋[1]、陳正宗[1,2]
[1]國立臺灣海洋大學河海工程學系
[2]國立臺灣海洋大學機械與機電工程學系
E-mail:m97520026@mail.ntou.edu.tw

國科會計劃編號:
NSC98-2221-E-019-017-MY3

摘要

本文使用可視為一種特別的基本解法的映像法來推導格林函數的解析解與半解析解。求解問題包含同心圓環、半平面含圓洞與偏心圓環的格林函數問題，及偏心圓環的邊界值問題。在同心圓環例子中，可用映像法推導出解析解。針對半平面含圓洞及偏心圓環的格林函數問題，可利用映像法的觀念透過滿足邊界條件就可決定最後兩個凝固點的源強度與常數項大小進而推導出半解析解。我們發現映像點映射到最後凝固的位置座落於雙極座標上的兩個焦點上。針對偏心圓環不含集中力的邊界值問題，我們以基本解法求解並與解析解比較作出誤差分佈圖，進而探討可能的源最佳佈點位置。基本解法的源最佳佈點位置可用映像法的觀念來尋找。而佈點位置如果包含到兩個焦點時，我們可以得到比較準確的結果。除此之外，基本解法中是否需要自由常數項也一併作討論。求解的結果與解析解相比得到很好的結果。

關鍵詞：基本解法、映像法、格林函數、邊界值問題。